ACS APPLIED MATERIALS & INTERFACES

www.acsami.org

Research Article

Self-Powered Gas Sensor Based on a Photovoltaic Cell and a Colorimetric Film with Hierarchical Micro/Nanostructures

Kyungnam Kang, Jaeho Park, Byeongsu Kim, Kwangmin Na, Incheol Cho, Junsuk Rho, Daejong Yang,* Jung-Yong Lee,* and Inkyu Park*

Cite This: *ACS Appl. Mater. Interfaces* 2020, 12, 39024–39032

Read Online

ACCESS | Metrics & More | Article Recommendations | Supporting Information

ABSTRACT: We report a new type of self-powered gas sensors based on the combination of a colorimetric film with hierarchical micro/nanostructures and organic photovoltaic cells. The transmittance of the colorimetric film with micro/nanostructures coated with *N*,*N*,*N*′,*N*′-tetramethyl-*p*-phenylenediamine (TMPD) changes by reacting with NO_2 gas, and it is measured as a current output of the photovoltaic cell. For this purpose, materials for the organic photovoltaic cells were carefully chosen to match the working wavelength of the TMPD. Micropost arrays and nanowires increase the surface area for the gas reaction and thus improve the transmittance changes by NO_2 gas (6.7% change for the plain film vs 27.7% change for the film with hierarchical micro/nanostructures to 20 ppm of NO_2). Accordingly, the colorimetric device with the hierarchical structures showed a response of $\Delta I/I_0$ = 0.27−20 ppm of NO_2, which is a 71% improvement compared to that of the plain sensing film. Furthermore, it showed a high selectivity against other gases such as H_2S and CO with almost negligible responses. Since the current output change of the photovoltaic cell is utilized as a sensor signal, no extra electrical power is required for the operation of gas sensors. We also integrated the sensor device with an electrical module and demonstrated a self-powered gas alarm system.

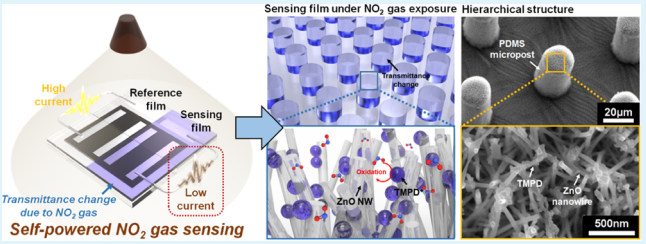

KEYWORDS: *colorimetric sensor, self-powered sensor, photovoltaic cell, gas sensor, micro/nanostructures, NO_2 sensor*

Recently, the importance of ubiquitous environmental monitoring has increased; therefore, the demand for air quality measurements such as indoor/outdoor air pollution and gas leakage in the industrial sites is also increasing.[1−3] Accordingly, many portable gas sensors are being utilized to measure air pollutants in daily life and work environment.[1,2,4−6] Among various types of gas sensors such as electrochemical,[7,8] chemoresistive,[9−15] optical,[16] and photoionization detectors,[17] the chemoresistive gas sensors based on the metal oxide have been most widely studied because of their excellent sensing characteristics such as high sensitivity, rapid response, low cost, small size, and a simple operating principle. In spite of these advantages, their applications in portable devices have been limited because of high electrical power for high-temperature operations. Even in the case of microelectromechanical system (MEMS) platform gas sensors, several tens of milliwatts (mW) are consumed for the sensor operation.[18−20] Meanwhile, optical gas sensors have also been used for gas monitoring systems. They identify gas types and concentrations by analyzing the absorbance or spectrum of the target gas.[16,21] However, they are also not suitable for portable gas sensors because of bulky size, high cost, and high power consumption.

To address these power issues of conventional gas sensors, self-powered gas sensors based on piezoelectric and triboelectric materials[22−24] and gas-sensitive colorimetric materials have been introduced. Piezoelectric or triboelectric self-powered gas sensors generate electrical power via a physical deformation or contact, and their output current changes by target gas exposure. However, practical applications of those gas sensors are limited because they require constant and continuous motions for real-time gas detection.[24] Colorimetric materials change their color or light transmittance by reacting with target gas.[25−28] Most of them are employed in the form of test papers and the color transition is noticeable by the naked eye.[28] Nevertheless, to convert the color change into quantitative data, high-cost image sensors[27] or high-power photodiodes are required.[29,30] For example, Courbat et al. reported a colorimetric gas sensor system composed of a light source, a photodetector, and an optical waveguide with embedded colorimetric materials.[29,30] However, it required large electrical power for the light source (<70 mW) and the

Received: May 3, 2020
Accepted: July 4, 2020
Published: July 4, 2020

https://dx.doi.org/10.1021/acsami.0c08128
ACS Appl. Mater. Interfaces 2020, 12, 39024−39032

photodetector (<150 mW) to overcome the energy loss in the waveguide.

In this study, we have developed a novel self-powered gas sensing mechanism by combining a colorimetric sensing film with hierarchical micro/nanostructures and an organic photovoltaic cell (Figure 1b). The transmittance of the colorimetric

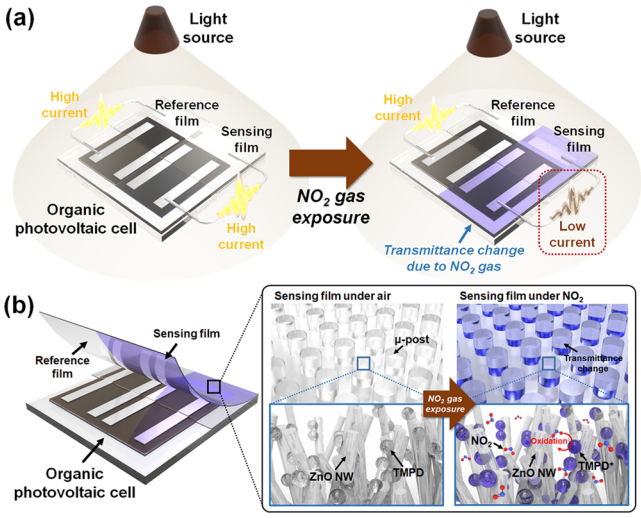

Figure 1. (a) Schematic illustration of the self-powered gas sensor consisting of a colorimetric film with hierarchical micro/nanostructures and an organic photovoltaic cell. The gas concentration is detected by comparing the light intensity passing through the sensing layer and the reference layer using the underlying photovoltaic cell. (b) Schematic image of the components of the self-powered gas sensor and the hierarchical micro/nanostructures for the enhancement of sensor performance. Nitrogen dioxide (NO_2) oxidizes *N*,*N*,*N*′,*N*′-tetramethyl-*p*-phenylenediamine (TMPD) on the sensing layer, which reduces the optical transmission of the layer.

sensing film changes by the reaction with target gas molecules. The photovoltaic cell located beneath the colorimetric sensing film measures the intensity of transmitted light, and this can be used to estimate the concentration of target gas (Figure 1a). Here, we have utilized cost-effective organic photovoltaic cells, in which the photovoltaic material was carefully selected to maximize the sensor response toward the specific colorimetric material used for the sensing film. This sensor system can be operated by ambient light sources from solar light for an outdoor application to a light-emitting diode (LED) for an indoor application, which shows the usefulness of our self-powered gas sensing system in various practical applications.

RESULTS AND DISCUSSION

The sensor device consists of the organic photovoltaic cell and the colorimetric sensing film with hierarchical micro/nanostructures. The concentration of gas is estimated by measuring the transmittance of this sensing layer. *N*,*N*,*N*′,*N*′-tetramethyl-*p*-phenylenediamine (TMPD) is a well-known colorimetric material for NO_2 gas.[31,32] When TMPD is exposed to NO_2, TMPD molecules are cationized to $TMPD^+$, while *para*-phenylenediamine (PPD, $C_6H_8N_2$) releases electrons. Oxidized TMPD coexists in the form of two resonance modes; some $TMPD^+$ can be further oxidized to $TMPD^{2+}$ by releasing secondary electrons under high concentrations of NO_2 gas. This oxidation reaction turns TMPD into a blue color, and TMPD is called Wurster's blue because of this phenomenon (Figure S1).[31−34] Since this color change is caused by the alteration of absorbance spectra, the concentration of NO_2 can be calculated by measuring the transmittance of the TMPD substrate.

Organic photovoltaic cells have been widely used for wearable and portable devices because of their mechanical flexibility, light-weight, low-cost, and simple fabrication process.[35] In addition, the absorption spectra of the organic photovoltaic cells are tunable by changing the composition or thickness of the materials. The organic photovoltaic cell, which was utilized as a light detector, was fabricated, as shown in Figure 2a. A single photovoltaic cell is composed of multiple layers including indium tin oxide (ITO, electrode), ZnO (electron transport layer), P3HT:PCBM (photoactive layer), MoO_3 (hole transport layer), and Ag (electrode). Among various candidates for the photoactive layer with high absorption under ambient light and high power conversion efficiency such as poly[[4,8-bis[(2-ethylhexyl)oxy]benzo[1,2-*b*:4,5-*b*′]dithiophene-2,6-diyl][3-fluoro-2-[(2-ethylhexyl)-carbonyl]thieno[3,4-*b*]thiophenediyl]] (PTB7), poly[4,8-bis-(5-(2-ethylhexyl)thiophen-2-yl)benzo[1,2-*b*;4,5-*b*′]-dithiophene-2,6-diyl-*alt*-(4-(2-ethylhexyl)-3-fluorothieno[3,4-*b*]thiophene-)-2-carboxylate-2-6-diyl] (PTB7-Th) and poly(3-hexylthiophene-2,5-diyl) (P3HT),[36] P3HT was chosen because of the highest light absorption rate in the working wavelength of the TMPD colorimetric film. In detail, the absorption spectra of PTB7, PTB7-Th, and P3HT were calculated by numerical simulations using transfer matrix formalism (TMF) (see the details about numerical simulations for absorption spectra and thickness optimization in the Supporting Information). Figure 2b presents the light absorption spectra of these three photoactive materials. Among these, P3HT showed the largest average absorbance of about 79.68% in the wavelength range of 380−650 nm, which matches well with the working wavelength of the TMPD film, as shown in Figure 2b,f. Figure 2c shows numerically calculated responses of the organic photovoltaic cells considering the absorption rate of photoactive materials and transmittance of the colorimetric sensing film with hierarchical micro/nanostructures under NO_2 gas. The response can be calculated as the relative change of short-circuit current density of the photovoltaic cell by NO_2 gas (J_{sc}) with respect to the initial short-circuit current density (J_{SC0}).[37] The responses of three different kinds of photoactive materials were calculated by changing the thickness of materials from 50 to 250 nm. The response of P3HT was in the range of 9.12−9.58%, which is larger than the two other materials for the entire thickness (50−250 nm) and the largest value was 9.58% at a thickness of 200 nm. This result verified that P3HT with a 200 nm thickness is the most effective material as the photoactive layer.

For the enhancement of sensing performance, a microstructure was formed on the surface of the PDMS substrate to increase the reaction sites of NO_2 gas. To investigate the effect of the microstructure on the sensing performance, the PDMS substrates with the aspect ratios of 1:1 (diameter = 20 μm and height = 20 μm) and 3:1 (diameter = 20 μm and height = 60 μm) were prepared using photolithography and a molding process on the micropatterned SU-8 templates (Figure 2d,e). The transmittances of TMPD-coated PDMS substrates before and after NO_2 exposure (20 ppm, 30 min) were measured. The transmittances of the PDMS substrates were more than 93.4% in the UV and visible light regions (300−800 nm), regardless of the presence or absence of the micropost array (solid lines

https://dx.doi.org/10.1021/acsami.0c08128
ACS Appl. Mater. Interfaces 2020, 12, 39024−39032

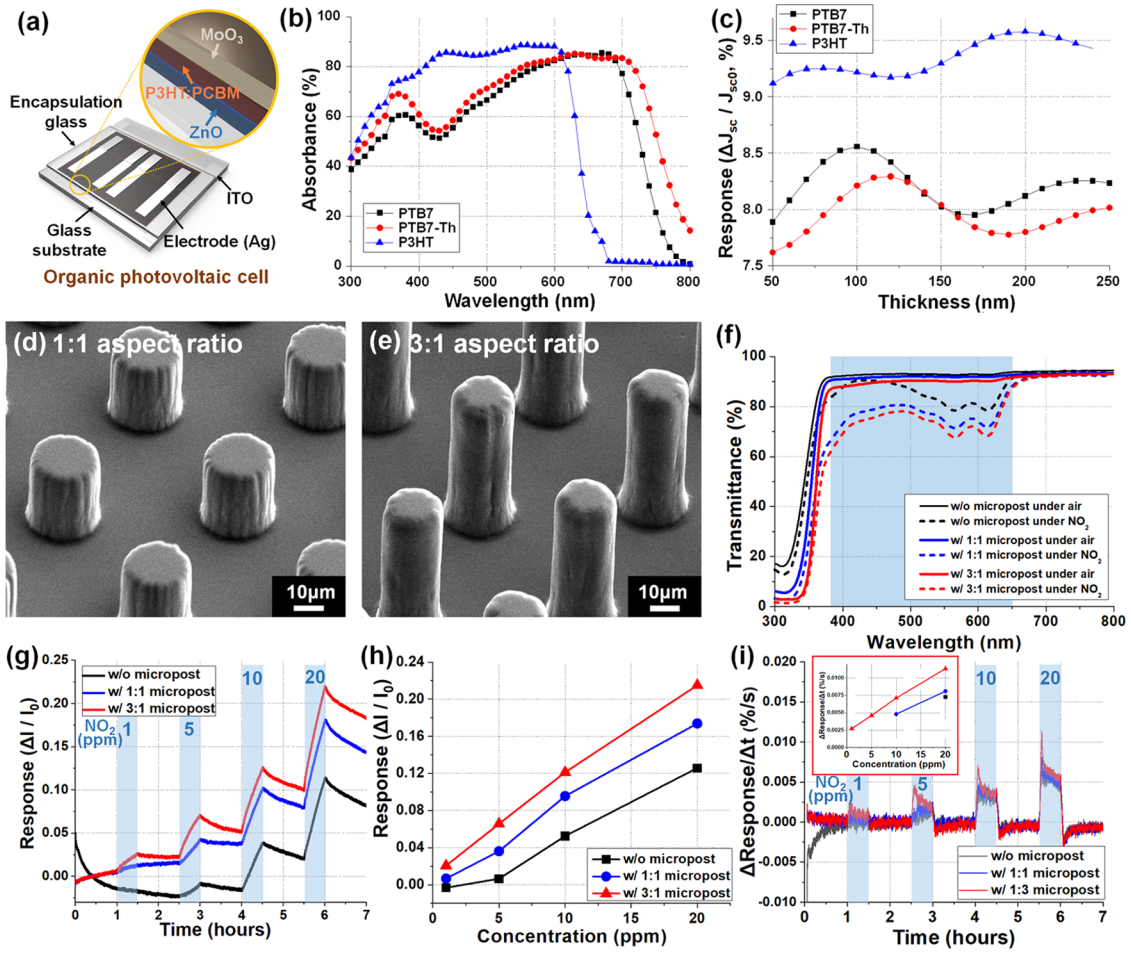

Figure 2. (a) Three-dimensional (3D) schematic of the organic photovoltaic cell consisting of the electron transport layer, photoactive layer, hole transport layer, and electrodes. (b) Absorption spectra of three kinds of photoactive materials (PTB7, PTB7-Th, and P3HT) used for the photovoltaic cell in the ultraviolet (UV) and visible light regions. (c) Numerically calculated responses of the photovoltaic cells considering the absorption rate of photoactive materials and transmittance of the colorimetric film under NO_2 gas. Scanning electron microscopy (SEM) images of (d) 1:1 aspect ratio micropost array and (e) 3:1 aspect ratio micropost array. (f) Transmittance of TMPD-coated poly(dimethylsiloxane) (PDMS) substrates before and after NO_2 exposure (20 ppm, 30 min), (g) sensing response under various NO_2 gas concentrations of the sensing film without and with the micropost array (1:1 and 3:1 ratio), and (h) NO_2 gas sensing performance of three types of sensing layers. (i) Time derivatives of sensing response under NO_2 gas and corresponding peak values of three types of sensing layers (inset).

in Figure S2a). When the PDMS substrates were exposed to 20 ppm of NO_2 gas for 30 min, the transmittance was almost the same with a change of less than 0.37% (dashed lines in Figure S2a). This means that there was no reaction between PDMS and NO_2 gas. To verify the gas sensing characteristics of TMPD, we measured the transmittance of microstructured PDMS with TMPD coating. As shown in the solid lines in Figure 2f, the transmittances of the TMPD-coated sensing layers were maintained around 91.8% in the visible light region (380−700 nm). When the TMPD-coated sensing layers were exposed to 20 ppm of NO_2 gas, their transmittances were dramatically decreased (dashed lines in Figure 2f). In the case of the plain PDMS substrate, the overall transmittance in the wavelength from 380 to 700 nm was decreased from 93.1 to 86.4%. Moreover, the transmittances of micropost arrays with aspect ratios of 1:1 and 3:1 were decreased from 92.0 to 78.7% and from 90.2 to 76.1%, respectively. Since the reaction between TMPD and NO_2 gas occurs on the surface of the sensing layers, the increased surface area by the micropost array contributes to a greater decrease of the transmittance of the sensing layer.

Figure 2g,h shows the responses of three kinds of colorimetric sensing films (without the micropost, with the micropost (1:1, 3:1 ratio)) to 1, 5, 10, and 20 ppm of NO_2 gas. The response is defined as $\Delta I/I_0$, where ΔI and I_0 represent the electric current change of the organic photovoltaic cell by the target gas and the initial electric current of the photovoltaic cell in ambient air, respectively. At the start of measurement in the colorimetric sensing film without the micropost, which was the first measurement with the organic photovoltaic cell, there was a continuous decrease of current output since it took some time for the photovoltaic cell to stabilize. However, this current output was finally stabilized and no more drift was found for other experiments. The substrates with the micropost array exhibited higher responses than the plain substrate and the response increased as the height of micropost increased. Therefore, the long micropost (3:1 ratio) showed the highest response due to the large surface area, and it was used for further experiments. The response to 10 ppm of NO_2 was improved by 130.8% as compared with the plain substrate. It should be noted that the sensor responses are not saturated during the period of target gas injection, and thus, the response

https://dx.doi.org/10.1021/acsami.0c08128
ACS Appl. Mater. Interfaces 2020, 12, 39024−39032

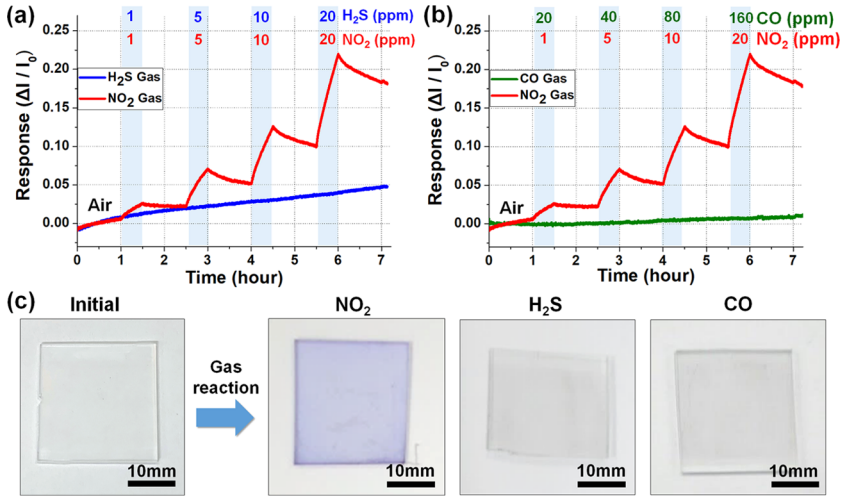

Figure 3. Dynamic sensing response of the colorimetric gas sensor to various concentrations of NO_2, (a) H_2S, and (b) CO gases for the selectivity test. (c) Photo images of the sensing layer before and after exposure to NO_2, H_2S, and CO gases.

and recovery times are very long. This slow response is mainly attributed to the diffusion-limited reaction of NO_2 gas inside the solid TMPD particles because the diffusion of gas (NO_2) into the solid phase (TMPD) tends to be slow, which is a common problem in colorimetric or vapochromic sensors.[38] Therefore, the time derivatives of the response curves can be utilized as an alternative to the response itself so that the gas detection can take much shorter time. As shown in Figure 2i, during the period of gas exposure, the time derivatives of the sensing responses rapidly increased to peak values, which was larger for higher gas concentrations. For example, in the sensing film with the micropost array (3:1 ratio), the time derivatives of the sensing responses were 0.0027, 0.0046, 0.0071, and 0.011%/s for 1, 5, 10, and 20 ppm of NO_2 concentrations, respectively. When the colorimetric film was oxidized by NO_2 gas and recovered in the ambient air environment, the colorimetric sensing film was not fully recovered as transparent to its initial state (data not shown). However, this limitation can be solved using the colorimetric sensing film as a disposable and replacing the colorimetric film after the alarm of NO_2 gas. Since there are various toxic gases in the atmosphere, it is important to minimize the effects of other interfering gases. The sensor responses to H_2S gas with concentrations of 1, 5, 10, and 20 ppm and CO gas with concentrations of 20, 40, 80, and 160 ppm were measured to examine the selectivity of the sensor. As shown in Figure 3a,b, the output current from the sensor rarely changed by both H_2S and CO gases. The colorimetric sensing film exposed to 20 ppm of NO_2 turned into a blue color, but the sensing layers exposed to 20 ppm of H_2S and 160 ppm of CO were still transparent with no apparent color change (Figure 3c). These results verify that this colorimetric sensor is highly selective to NO_2 gas due to the selective reactivity of TMPD with a particular target gas, NO_2.

For practical applications, the sensors are required to operate using ambient light as a power source. First, the effect of the illumination conditions (collimated light vs diffused light) on the sensing response was investigated. As shown in Figure S3, no statistically significant difference between collimated and diffused light conditions could be observed. Therefore, it could be concluded that various light sources can be utilized as the power source, no matter if it is collimated or diffused light. To demonstrate the sensor operation under various ambient light conditions in the outdoor and indoor environments, a solar illuminator and an LED lamp were used as light sources. The sunlight intensity at the sea level on a clear day is 1000 W/m^2.[39] Accordingly, the simulated solar light with intensities of 126−779 W/m^2 were used as light sources. As shown in Figure S4a, the sensor showed responses to NO_2 gas from low light intensity (126 W/m^2) to high light intensity (779 W/m^2). It is observed that the sensor response decreases with increasing light intensity, regardless of the gas concentrations (Figure S4b). This response decrease may be caused by photoionization of TMPD toward $TMPD^+$ induced by the irradiation of ultraviolet (UV) ray during the experiments. It has been reported that TMPD has a high absorption spectrum with peaks at 260 nm, and it can be readily photoionized into $TMPD^+$ under UV irradiation.[40,41] The ambient light source used in this study irradiated some amount of UV ray even though an optical filter for the visible light range was used (UV intensity at the wavelength of 254 nm in used visible light = 0.97 W/m^2 under irradiation of visible light with 780 W/m^2, data not shown). As a result, the TMPD molecules are oxidized by both NO_2 gas and UV ray, and thus, the corresponding response to NO_2 gas is reduced under higher light intensities. This limitation of TMPD will not be critical in real applications because UV ray in the range of 260 nm from sunlight is almost negligible on the earth's surface.[42] Furthermore, the change of sensor response by the illumination condition can be compensated by monitoring the intensity of light source with a reference photovoltaic cell, which is demonstrated later in Figure 5. An LED with an intensity of 19 W/m^2 was also used as a light source for the sensor to verify that the sensor can operate under a dim indoor lighting condition. As shown in Figure S4c,d, the sensor exhibited high sensitivity to NO_2 under low light intensities.

To enhance the gas sensing performance, hierarchical micro/nanostructures were further fabricated for increasing the surface area of the colorimetric sensing material. ZnO nanowires (NWs) were synthesized on the surface of microposts using a hydrothermal reaction. Figure 4a,b shows the SEM images of ZnO NWs integrated on the micropost array. Here, ZnO NWs with lengths of ~1 μm and diameters of ~50 nm were synthesized on the microposts and this

https://dx.doi.org/10.1021/acsami.0c08128
ACS Appl. Mater. Interfaces 2020, 12, 39024−39032

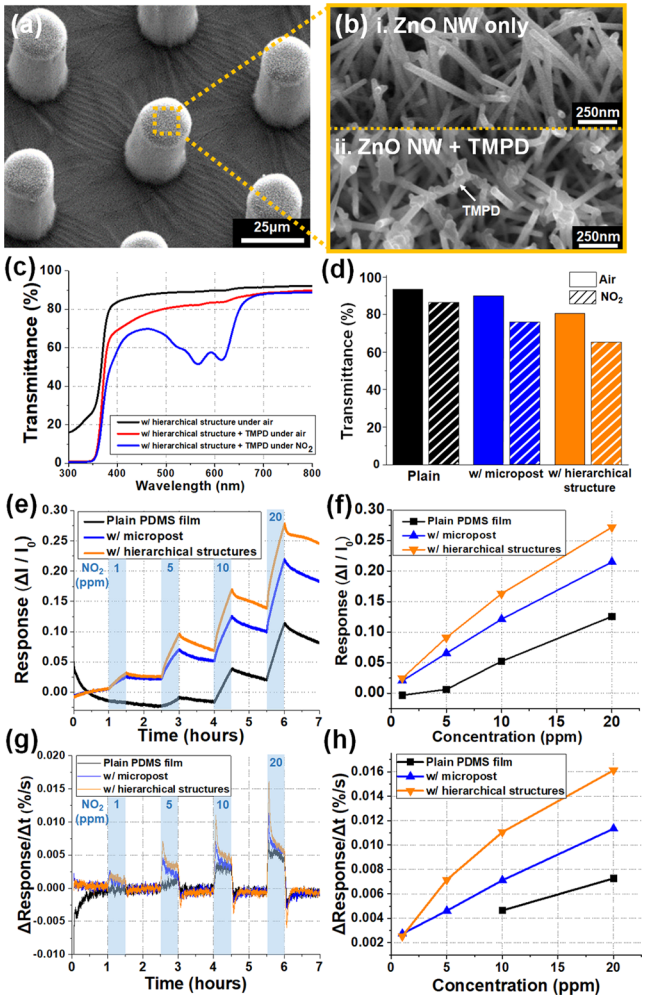

Figure 4. (a) SEM images of the ZnO nanowire-integrated micropost array (hierarchical micro/nanostructures) and (b) higher-magnification image of integrated ZnO nanowires (b-i) without and (b-ii) with TMPD coating. (c) Transmittance of the PDMS film with hierarchical structures before and after coating with TMPD under air and 20 ppm of NO_2 gas. (d) Comparison of transmittance change of three kinds of the colorimetric films with or without micro/nanostructures before and after NO_2 exposure. (e) Dynamic sensing response and (f) concentration vs response curve of the colorimetric layer with and without the micropost array and hierarchical micro/nanostructures to various concentrations of NO_2 gas. (g) Time derivative of sensing response under NO_2 gas. (h) Peak value of the time derivative of sensor response under various NO_2 gas concentrations.

allowed for a significant increase of the surface area. Figure 4c shows the transmittance spectra of the ZnO NW-integrated micropost array (black line) and the TMPD-coated, ZnO NW-integrated micropost array in air (red line) and in 20 ppm of NO_2 gas (blue line) environments. The transmittance of ZnO NW-integrated substrates was significantly decreased in the UV region due to the band gap of ZnO (3.3 eV).[43] However, it was maintained above 88.4% in the visible light region (380−700 nm) and ZnO did not change the transmittance of the film under the exposure of NO_2 gas, as shown in Figure S2b. The transmittance of the TMPD-coated sensing film with the hierarchical micro/nanostructures was 80.3% in the visible light region (wavelength of 380−700 nm), and it decreased to 65.4% by 20 ppm of NO_2 gas. Figure 4d summarizes the transmittance change of plain PDMS, the PDMS substrate with the micropost array, and the PDMS substrate with the hierarchical micro/nanostructures. As the surface area is increased by microposts and ZnO NWs, larger change of transmittance occurs. Figure 4e shows the dynamic sensing response of the colorimetric sensing film with and without microposts and ZnO NWs. By increasing the concentration of NO_2 gas, the transmittance of the colorimetric sensing film with the hierarchical micro/nanostructures decreased and thus the output currents of the photovoltaic cell also decreased. The responses of the sensing film with microposts were 0.021, 0.066, 0.12, and 0.22 to 1, 5, 10, and 20 ppm of NO_2 gas, respectively. The response was increased by ∼70.8% as compared to the plain sensing film for 20 ppm of NO_2. In addition, the responses of the sensing film with the hierarchical micro/nanostructures were 0.025, 0.091, 0.16, and 0.27 under 1, 5, 10, and 20 ppm of NO_2 gas, respectively. The responses were additionally increased by ∼26.5% as compared to the sensing film with the microposts but without ZnO NWs for 20 ppm of NO_2 (Figure 4f). In the case of the time derivatives of sensing responses, the peak values in the sensing film with hierarchical micro/nanostructures were 0.0025, 0.0072, 0.011, 0.016%/s to 1, 5, 10, 20 ppm of NO_2 gas, respectively (Figure 4g,h). The sensing film with hierarchical micro/nanostructures shows the biggest time derivatives. In the case of the sensing film without any micro/nanostructures, the peak values were difficult to be calculated, especially in lower gas concentrations (<10 ppm). This result verifies that the formation of the hierarchical micro/nanostructures increases the surface area for the gas reaction and thus enhances the sensor response. Furthermore, for quantifying the gas concentration more quickly, the time derivatives of the sensor response can be utilized, and the hierarchical structures can significantly enhance and contribute to the usability of the time derivatives.

Figure 5a,b shows the demonstration of the self-powered gas sensor system in an indoor environment. The self-powered gas sensing device composed of a hierarchical micro/nanostructured colorimetric sensing film and an organic photovoltaic cell was connected to an electric circuit consisting of an operational amplifier (op-amp), a commercial solar cell, a red LED, etc. A single photovoltaic cell consisted of five subphotovoltaic cells, as shown in Figure 5a. Among the five subphotovoltaic cells, two cells were covered by the sensing film, which had TMPD-coated hierarchical micro/nanostructures, and the photocurrent through these two cells detected the change of light intensity by NO_2 gas. Another two cells were covered by the reference film, which had the hierarchical micro/nanostructures without TMPD coating, and the photocurrent through these two cells was used as a reference. Using this configuration and subtracting the photocurrent at the reference cells from that at the sensing cells, the error of the organic photovoltaic cell such as the change of ambient light intensity or the drift effect shown in Figure 2g could be easily compensated. The terminals were connected to the op-amp, and the commercial photovoltaic cell was used to generate the driving power for the op-amp and red LED. A white LED lamp for office use was utilized as the light source for the sensor system to operate. For the electronic circuitry of the self-powered gas sensor system, the circuitry should be composed of electronic components as little as possible to minimize the power consumption rather than using various active components and integrated circuits (ICs). Therefore, a comparator circuit, which requires only one op-amp, was designed to turn on/off the red LED for an alarm system. The

https://dx.doi.org/10.1021/acsami.0c08128
ACS Appl. Mater. Interfaces 2020, 12, 39024−39032

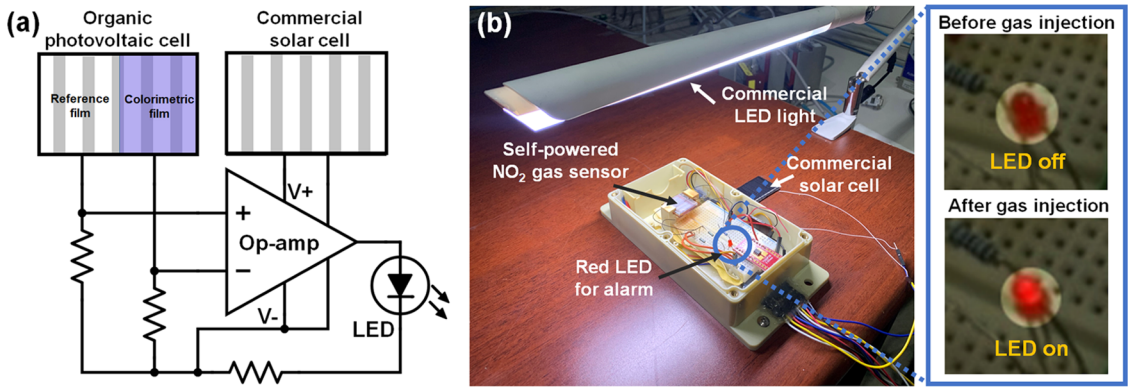

Figure 5. Demonstration of the self-powered gas sensor system in an indoor environment: (a) schematics of electronic circuits for the self-powered gas sensor with an LED alarm. (b) Experimental image of the NO_2 gas alarm system based on the self-powered gas sensor (inset images: LED off under air and LED on under a NO_2 gas environment. A red LED was turned on by 20 ppm of NO_2 gas).

voltage difference between the noninverting input (V+) and the inverting input (V−) of op-amp caused by the current difference between the sensing and reference cells was amplified. When the amplified voltage at the output terminal of the op-amp reached the threshold voltage of the LED, the red LED was turned on to indicate a gas alarm.

The concentration of NO_2 gas for alarming was set at 20 ppm by adjusting the resistance of variable resistors. Figure 5b and the inset image show the actual demonstration of the self-powered gas sensor based on the above-mentioned configuration. In air condition, the reference cell and the sensing cell generated similar output currents, so that the output voltage of the op-amp was below the threshold voltage and the red LED was turned off. When NO_2 gas was injected into the sensing system, the output current of the sensing cell continuously decreased, while that of the reference cell kept constant. As a consequence, the output voltage of the op-amp exceeded the threshold voltage, and the red LED was turned on, as shown in the inset image of Figure 5b. Therefore, this self-powered gas sensing system could inform the existence of NO_2 gas by alarming through the red LED. Based on this demonstration, we could confirm that the proposed self-powered gas sensing system can operate in a weak indoor light environment without any external power.

CONCLUSIONS

We have developed a self-powered gas sensor using an organic photovoltaic cell and a hierarchical micro/nanostructure coated with a colorimetric material. When the TMPD-coated sensing film is exposed to NO_2 gas, the transmittance of TMPD in the wavelength of 380−650 nm is decreased and the intensity change of light passing through the colorimetric sensing film is detected by the underlying organic photovoltaic cell, whose working wavelength is carefully designed to match the transmission spectra of TMPD. To enhance the gas sensing performance, hierarchical micro/nanostructures consisting of a micropost array and ZnO NWs were applied to the sensing film to increase the surface area. This hierarchical structure allowed for a significant enhancement of the sensor response to NO_2 gas. The sensor showed good sensing performance to 1−20 ppm of NO_2 gas with high selectivity against other interfering gases. Finally, the self-powered gas sensing system could operate using an indoor light source only for both powering the sensor system and measuring the sensor response. As mentioned in the beginning, the needs of gas sensing are rapidly increasing because of increased air pollution and strengthened environmental regulation. However, powering the gas sensing system has been a big hurdle for the gas sensor network due to high power consumption of the gas sensor. Therefore, we highly expect that the proposed self-powered gas sensing system, combining the photovoltaic cell and colorimetric sensing film, can be a useful solution for future environmental monitoring applications. Furthermore, this concept can be adapted to other types of physical and chemical sensors by offering a solution for the power-related issue, which will be a highly demanded requirement in the near future of sensor networks and the internet of things (IoT).

MATERIALS AND METHODS

Fabrication of the Organic Photovoltaic Cell. Indium tin oxide (ITO, thickness = 75 nm)-coated glass substrates (single side coated, 25.4 mm × 25.4 mm, JM International Co., South Korea) were prepared for the substrate and electrodes. Zinc acetate dihydrate (1 g, Sigma-Aldrich) and ethanolamine (0.28 g, Sigma-Aldrich) were dissolved in 2-methoxyethanol (10 mL, Sigma-Aldrich) and stirred over 8 h at room temperature. The solution was spin-coated on the ITO-coated glass substrate at 3000 rpm for 30 s and heated at 200 °C for 30 min in a furnace to fabricate an electron transport layer.[44] Then, a mixture of poly-3-hexylthiophene-2,5-diyl (P3HT, Rieke metals) and phenyl-C_{61}-butyric acid methyl ester (PCBM, Nano-C Company) at a ratio of 1:1 was dissolved as a concentration of 10 mg/ml in a solvent mixed with *o*-dichlorobenzene (DCB, Sigma-Aldrich) and 1,8-diiodooctane (DIO, Sigma-Aldrich) at a ratio of 97:3. The solution was spin-coated on the substrate at 2000 rpm for 60 s and heated at 150 °C for 10 min in a furnace to fabricate a photoactive layer.[45] Then, a 10 nm thick molybdenum oxide (MoO_3) layer and a 150 nm thick patterned silver (Ag) layer were deposited by thermal evaporation as a hole-transporting layer and electrodes, respectively. After the fabrication of the photoactive layer, it was further encapsulated with a commercial thick slide glass (thickness = 1 mm) using an optical adhesive (Norland Optical Adhesive 63, Norland Products) to avoid exposure of the photoactive layer to the outer environment.

Fabrication of the Colorimetric Sensing Film with Micro/Nanostructures. SU-8 (MicroChem) molds for the micropost array were fabricated by the conventional photolithography process. The micropost array was designed to be 20 μm in diameter, 20 or 60 μm in height, and 40 μm in gap between the microposts. PDMS (Sylgard 184, Dow) was cast over the SU-8 molds and cured at 75 °C for 2 h to form a 1.5 mm thick sample with a micropost array. Therefore, the replicated PDMS contained both the micropost and substrate as a one-body structure, which did not require a further assembly or bonding process between the micropost and the PDMS substrate. To fabricate a hierarchical micro/nanostructure with ZnO nanowires

https://dx.doi.org/10.1021/acsami.0c08128
ACS Appl. Mater. Interfaces 2020, 12, 39024−39032

(NW) integrated on the micropost array, an additional ZnO NW synthesis process was carried out. The ZnO seed layer with a target thickness of 5 nm was deposited on the PDMS micropost array using a sputtering process of the ZnO target, and ZnO NWs were synthesized on the surface of the PDMS micropost using the hydrothermal reaction.[18] The colorimetric material consisted of 0.5 g of *N*,*N*,*N*′,*N*′-tetramethyl-*p*-phenylenediamine (TMPD, Sigma-Aldrich) and 20 mL of isopropyl alcohol (IPA, Avantor). A spray gun with the colorimetric material solution was placed 30 cm away from the PDMS substrate. The sensing materials were spray-coated for 30 s on three different substrates (a plain PDMS substrate, a PDMS substrate with the micropost array, and a PDMS substrate with hierarchical micro/nanostructures) for comparison of sensing performances.

Optical Characterization of the Colorimetric Sensing Film with Micro/Nanostructures. A UV−vis spectrophotometer (UV-2600Plus, Shimadzu, Japan) was utilized to measure the transmittance of the colorimetric sensing films. The transmittance of different samples (a plain PDMS substrate, a PDMS substrate with a micropost array (1:1 and 3:1 aspect ratios), and a PDMS substrate with hierarchical micro/nanostructures) without colorimetric layers were measured as references. The transmittances of these samples were also measured after TMPD−IPA coating and after exposure to 20 ppm of NO_2 gas, respectively.

Electrical Circuits for the Colorimetric Gas Sensor. The electrical circuit for the gas alarm system consists of an organic photovoltaic cell, a commercial photovoltaic cell (MSCA3040, Eleparts, South Korea), an operational amplifier (op-amp, LM7332, Texas Instruments), and a light-emitting diode (LED, BL-B5134, BRTLED, Taiwan). A single photovoltaic cell consists of five subphotovoltaic cells. Two subphotovoltaic cells were covered by the PDMS film without the colorimetric material (TMPD), and the other two subphotovoltaic cells were covered by the colorimetric sensing film with the hierarchical micro/nanostructures and TMPD coating. For the assembly of the colorimetric sensing film, the bottom plain side of the sensing film was attached to the surface of the organic photovoltaic cell that was encapsulated with a slide glass. On the other hand, the top side of the sensing film with the hierarchical structure and TMPD coating was exposed to the outer environment. These two organic photovoltaic cells were connected to the input terminals of the op-amp, and the output terminal of the op-amp was connected to the LED that provided a gas alarm. A commercial photovoltaic cell was connected to the power input port of the op-amp.

Measurement of Sensor Response to NO_2 Gas under Ambient Light. A xenon light source (LAX-C100, Asahi Spectra) was employed as an ambient light source. The sensor device was placed in a chamber with a transparent window, and various concentrations (1, 5, 10, and 20 ppm) of NO_2 gas were supplied to the chamber. The distance between the light source and the sensor device was 100 mm, and the intensity of the light source was fixed at 235 W/m^2. In the case of the sensor performance test under various light intensities, the light source with intensities of 126, 235, 410, 566, 659, and 779 W/m^2 were utilized. Since the light was originally emitted as a diffused light source, a collimator lens was utilized to compare the difference in sensor performance between the diffused and collimated light sources.

■ ASSOCIATED CONTENT

Supporting Information

The Supporting Information is available free of charge at https://pubs.acs.org/doi/10.1021/acsami.0c08128.

Chemical reaction of TMPD with NO_2 gas, numerical simulation for absorption spectra of different photoactive layers and thicknesses, transmittance of PDMS with different structures without TMPD coating, sensor responses to NO_2 with diffused and collimated light sources, and NO_2 gas sensing performance under various light intensities (PDF)

■ AUTHOR INFORMATION

Corresponding Authors

Daejong Yang − *Department of Mechanical and Automotive Engineering, Kongju National University, Cheonan 31080, Republic of Korea;* orcid.org/0000-0002-8774-5843; Email: daejong@kongju.ac.kr

Jung-Yong Lee − *School of Electrical Engineering, Korea Advanced Institute of Science and Technology (KAIST), Daejeon 34141, Republic of Korea;* orcid.org/0000-0002-5347-8230; Email: jungyong.lee@kaist.ac.kr

Inkyu Park − *Department of Mechanical Engineering, Korea Advanced Institute of Science and Technology (KAIST), Daejeon 34141, Republic of Korea;* orcid.org/0000-0001-5761-7739; Email: inkyu@kaist.ac.kr

Authors

Kyungnam Kang − *Department of Mechanical Engineering, Korea Advanced Institute of Science and Technology (KAIST), Daejeon 34141, Republic of Korea*

Jaeho Park − *Department of Mechanical Engineering, Korea Advanced Institute of Science and Technology (KAIST), Daejeon 34141, Republic of Korea;* orcid.org/0000-0002-0213-8076

Byeongsu Kim − *School of Electrical Engineering, Korea Advanced Institute of Science and Technology (KAIST), Daejeon 34141, Republic of Korea*

Kwangmin Na − *Graduate School of EEWS, Korea Advanced Institute of Science and Technology (KAIST), Daejeon 34141, Republic of Korea*

Incheol Cho − *Department of Mechanical Engineering, Korea Advanced Institute of Science and Technology (KAIST), Daejeon 34141, Republic of Korea*

Junsuk Rho − *Department of Mechanical Engineering and Department of Chemical Engineering, Pohang University of Science and Technology (POSTECH), Pohang 37673, Republic of Korea;* orcid.org/0000-0002-2179-2890

Complete contact information is available at: https://pubs.acs.org/10.1021/acsami.0c08128

Author Contributions

K.K. and J.P. contributed equally to this work. The manuscript was written through the contribution of all authors. All authors have given approval to the final version of the manuscript.

Notes

The authors declare no competing financial interest.

■ ACKNOWLEDGMENTS

This work was supported by the National Research Foundation of Korea (NRF) grant funded by the Korea Government (MSIT) (No. 2018R1A2B2004910) and KAI-NEET Institute (N11200058). J.R. acknowledges the Green Science Program funded by POSCO.

■ REFERENCES

(1) Bardana, E. J., Jr. Indoor Pollution and Its Impact on Respiratory Health. *Ann. Allergy, Asthma, Immunol.* **2001**, *87*, 33−40.

(2) Becker, T.; Mühlberger, S.; Braunmühl, C. B.-v.; Müller, G.; Ziemann, T.; Hechtenberg, K. V. Air Pollution Monitoring Using Tin-Oxide-Based Microreactor Systems. *Sens. Actuators, B* **2000**, *69*, 108−119.

(3) Kaushik, A.; Kumar, R.; Arya, S. K.; Nair, M.; Malhotra, B. D.; Bhansali, S. Organic-Inorganic Hybrid Nanocomposite-Based Gas

Sensors for Environmental Monitoring. *Chem. Rev.* **2015**, *115*, 4571−4606.
(4) Grünhage, L.; Dämmgen, U.; Haenel, H.-D.; Jäger, H.-J. Response of a Grassland Ecosystem to Air Pollutants. VI. The Chemical Climate: Concentrations and Potential Flux Densities of Relevant Criteria Pollutants. *Environ. Pollut.* **1998**, *101*, 215−220.
(5) Odlyha, M.; Foster, G. M.; Cohen, N. S.; Sitwell, C.; Bullock, L. Microclimate Monitoring of Indoor Environments Using Piezoelectric Quartz Crystal Humidity Sensors. *J. Environ. Monit.* **2000**, *2*, 127−131.
(6) Tao, W.-H.; Tsai, C.-H. H_2S Sensing Properties of Noble Metal Doped WO_3 Thin Film Sensor Fabricated by Micromachining. *Sens. Actuators, B* **2002**, *81*, 237−247.
(7) Xiong, L.; Compton, R. G. Amperometric Gas Detection: A Review. *Int. J. Electrochem. Sci.* **2014**, *9*, 7152−7181.
(8) Khan, M. A. H.; Rao, M. V.; Li, Q. Recent Advances in Electrochemical Sensors for Detecting Toxic Gases: NO_2, SO_2 and H_2S. *Sensors* **2019**, *19*, No. 905.
(9) Yang, D.; Kim, D.; Ko, S. H.; Pisano, A. P.; Li, Z.; Park, I. Focused Energy Field Method for the Localized Synthesis and Direct Integration of 1D Nanomaterials on Microelectronic Devices. *Adv. Mater.* **2015**, *27*, 1207−1215.
(10) Yang, D.; Kang, K.; Kim, D.; Li, Z.; Park, I. Fabrication of Heterogeneous Nanomaterial Array by Programmable Heating and Chemical Supply within Microfluidic Platform towards Multiplexed Gas Sensing Application. *Sci. Rep.* **2015**, *5*, No. 8149.
(11) Yang, D.; Fuadi, M. K.; Kang, K.; Kim, D.; Li, Z.; Park, I. Multiplexed Gas Sensor Based on Heterogeneous Metal Oxide Nanomaterial Array Enabled by Localized Liquid-Phase Reaction. *ACS Appl. Mater. Interfaces* **2015**, *7*, 10152−10161.
(12) Wang, C.; Yin, L.; Zhang, L.; Xiang, D.; Gao, R. Metal Oxide Gas Sensors: Sensitivity and Influencing Factors. *Sensors* **2010**, *10*, 2088−2106.
(13) Lim, M. A.; Kim, D. H.; Park, C. O.; Lee, Y. W.; Han, S. W.; Li, Z.; Williams, R. S.; Park, I. A New Route toward Ultrasensitive, Flexible Chemical Sensors: Metal Nanotubes by Wet-Chemical Synthesis along Sacrificial Nanowire Templates. *ACS Nano* **2012**, *6*, 598−608.
(14) Korotcenkov, G. Metal Oxides for Solid-State Gas Sensors: What Determines Our Choice? *Mater. Sci. Eng., B* **2007**, *139*, 1−23.
(15) Suh, J.-H.; Cho, I.; Kang, K.; Kweon, S.-J.; Lee, M.; Yoo, H.-J.; Park, I. Fully Integrated and Portable Semiconductor-Type Multi-Gas Sensing Module for IoT Applications. *Sens. Actuators, B* **2018**, *265*, 660−667.
(16) Hodgkinson, J.; Tatam, R. P. Optical Gas Sensing: A Review. *Meas. Sci. Technol.* **2013**, *24*, No. 012004.
(17) Spinelle, L.; Gerboles, M.; Kok, G.; Persijn, S.; Sauerwald, T. Review of Portable and Low-Cost Sensors for the Ambient Air Monitoring of Benzene and Other Volatile Organic Compounds. *Sensors* **2017**, *17*, No. 1520.
(18) Cho, I.; Kang, K.; Yang, D.; Yun, J.; Park, I. Localized Liquid-Phase Synthesis of Porous SnO2 Nanotubes on MEMS Platform for Low-Power, High Performance Gas Sensors. *ACS Appl. Mater. Interfaces* **2017**, *9*, 27111−27119.
(19) Kang, K.; Yang, D.; Park, J.; Kim, S.; Cho, I.; Yang, H. H.; Cho, M.; Mousavi, S.; Choi, K. H.; Park, I. Micropatterning of Metal Oxide Nanofibers by Electrohydrodynamic (EHD) Printing towards Highly Integrated and Multiplexed Gas Sensor Applications. *Sens. Actuators, B* **2017**, *250*, 574−583.
(20) Baranov, A.; Spirjakin, D.; Akbari, S.; Somov, A. Optimization of Power Consumption for Gas Sensor Nodes: A Survey. *Sens. Actuators, A* **2015**, *233*, 279−289.
(21) Bogue, R. Detecting Gases with Light: A Review of Optical Gas Sensor Technologies. *Sens. Rev.* **2015**, *35*, 133−140.
(22) Zhang, H.; Yang, Y.; Su, Y.; Chen, J.; Hu, C.; Wu, Z.; Liu, Y.; Wong, C. P.; Bando, Y.; Wang, Z. L. Triboelectric Nanogenerator as Self-Powered Active Sensors for Detecting Liquid/Gaseous Water/Ethanol. *Nano Energy* **2013**, *2*, 693−701.
(23) Zhao, Y.; Lai, X.; Deng, P.; Nie, Y.; Zhang, Y.; Xing, L.; Xue, X. Pt/ZnO Nanoarray Nanogenerator as Self-Powered Active Gas Sensor with Linear Ethanol Sensing at Room Temperature. *Nanotechnology* **2014**, *25*, No. 115502.
(24) Kim, J. H.; Chun, J.; Kim, J. W.; Choi, W. J.; Baik, J. M. Self-Powered, Room-Temperature Electronic Nose Based on Triboelectrification and Heterogeneous Catalytic Reaction. *Adv. Funct. Mater.* **2015**, *25*, 7049−7055.
(25) Schmitt, K.; Tarantik, K.; Pannek, C.; Wöllenstein, J. Colorimetric Materials for Fire Gas Detection—A Review. *Chemosensors* **2018**, *6*, No. 14.
(26) Janzen, M. C.; Ponder, J. B.; Bailey, D. P.; Ingison, C. K.; Suslick, K. S. Colorimetric Sensor Arrays for Volatile Organic Compounds. *Anal. Chem.* **2006**, *78*, 3591−3600.
(27) Lin, C.; Xian, X.; Qin, X.; Wang, D.; Tsow, F.; Forzani, E.; Tao, N. High Performance Colorimetric Carbon Monoxide Sensor for Continuous Personal Exposure Monitoring. *ACS Sens.* **2018**, *3*, 327−333.
(28) Cha, J.-H.; Kim, D.-H.; Choi, S.-J.; Koo, W.-T.; Kim, I.-D. Sub-Parts-per-Million Hydrogen Sulfide Colorimetric Sensor: Lead Acetate Anchored Nanofibers toward Halitosis Diagnosis. *Anal. Chem.* **2018**, *90*, 8769−8775.
(29) Courbat, J.; Briand, D.; Wöllenstein, J.; de Rooij, N. F. Polymeric Foil Optical Waveguide with Inkjet Printed Gas Sensitive Film for Colorimetric Sensing. *Sens. Actuators, B* **2011**, *160*, 910−915.
(30) Courbat, J.; Briand, D.; Damon-Lacoste, J.; Wöllenstein, J.; de Rooij, N. F. Evaluation of PH Indicator-Based Colorimetric Films for Ammonia Detection Using Optical Waveguides. *Sens. Actuators, B* **2009**, *143*, 62−70.
(31) Michaelis, L.; Schubert, M. P.; Granick, S. The Free Radicals of the Type of Wurster's Salts. *J. Am. Chem. Soc.* **1939**, *61*, 1981−1992.
(32) Schwarzenbacher, G.; Evers, B.; Schneider, I.; de Raadt, A.; Besenhard, J.; Saf, R. Investigation of 2,6-Disubstituted N,N,N′,N′-Tetramethyl-p-Phenylenediamines as Precursors/Building Blocks for Molecular Magnets. *J. Mater. Chem.* **2002**, *12*, 534−539.
(33) Ho, K.-C.; Fang, Y.-W.; Hsu, Y.-C.; Chen, L.-C. The Influences of Operating Voltage and Cell Gap on the Performance of a Solution-Phase Electrochromic Device Containing HV and TMPD. *Solid State Ionics* **2003**, *165*, 279−287.
(34) Kao, S.-Y.; Kawahara, Y.; Nakatsuji, S.; Ho, K.-C. Achieving a Large Contrast, Low Driving Voltage, and High Stability Electrochromic Device with a Viologen Chromophore. *J. Mater. Chem. C* **2015**, *3*, 3266−3272.
(35) Scharber, M. C.; Sariciftci, N. S. Efficiency of Bulk-Heterojunction Organic Solar Cells. *Prog. Polym. Sci.* **2013**, *38*, 1929−1940.
(36) Huang, H.; Yang, L.; Sharma, B. Recent Advances in Organic Ternary Solar Cells. *J. Mater. Chem. A* **2017**, *5*, 11501−11517.
(37) He, Z.; Zhong, C.; Huang, X.; Wong, W. Y.; Wu, H.; Chen, L.; Su, S.; Cao, Y. Simultaneous Enhancement of Open-Circuit Voltage, Short-Circuit Current Density, and Fill Factor in Polymer Solar Cells. *Adv. Mater.* **2011**, *23*, 4636−4643.
(38) Li, Z.; Askim, J. R.; Suslick, K. S. The Optoelectronic Nose: Colorimetric and Fluorometric Sensor Arrays. *Chem. Rev.* **2019**, *119*, 231−292.
(39) Contreras, M. A.; Egaas, B.; Ramanathan, K.; Hiltner, J.; Swartzlander, A.; Hasoon, F.; Noufi, R. Progress toward 20% Efficiency in $Cu(In,Ga)Se_2$ Polycrystalline Thin-Film Solar Cells. *Prog. Photovoltaics* **1999**, *7*, 311−316.
(40) Holroyd, R. A.; Russell, R. L. Solvent and Temperature Effects in the Photoionization of Tetramethyl-p-Phenylenediamine. *J. Phys. Chem. A.* **1974**, *78*, 2128−2135.
(41) Albrecht, A. C.; Simpson, W. T. Spectroscopic Study of Wurster's Blue and Tetramethyl-p-Phenylenediamine with Assignments of Electronic Transitions. *J. Am. Chem. Soc.* **1955**, *77*, 4454−4461.
(42) D'Orazio, J.; Jarrett, S.; Amaro-Ortiz, A.; Scott, T. UV Radiation and the Skin. *Int. J. Mol. Sci.* **2013**, *14*, 12222−12248.

https://dx.doi.org/10.1021/acsami.0c08128
ACS Appl. Mater. Interfaces 2020, 12, 39024−39032

(43) Srikant, V.; Clarke, D. R. On the Optical Band Gap of Zinc Oxide. *J. Appl. Phys.* **1998**, *83*, 5447−5451.
(44) Cha, H. C.; Huang, Y. C.; Hsu, F. H.; Chuang, C. M.; Lu, D. H.; Chou, C. W.; Chen, C. Y.; Tsao, C. S. Performance Improvement of Large-Area Roll-to-Roll Slot-Die-Coated Inverted Polymer Solar Cell by Tailoring Electron Transport Layer. *Sol. Energy Mater. Sol. Cells* **2014**, *130*, 191−198.
(45) He, Y.; Shao, M.; Xiao, K.; Smith, S. C.; Hong, K. High-Performance Polymer Photovoltaics Based on Rationally Designed Fullerene Acceptors. *Sol. Energy Mater. Sol. Cells* **2013**, *118*, 171−178.

https://dx.doi.org/10.1021/acsami.0c08128
ACS Appl. Mater. Interfaces 2020, 12, 39024−39032